ACS OMEGA

Open Access

http://pubs.acs.org/journal/acsodf

Article

Nanostructured WS_2@Chitosan-Modified Screen-Printed Carbon Electrodes for Efficient Amperometric Detection of Histamine

Diksha Singh, Ankur Srivastava, Vivek K. Chaturvedi, and Jay Singh*

Cite This: *ACS Omega* 2025, 10, 3153−3164

Read Online

ACCESS | Metrics & More | Article Recommendations | Supporting Information

ABSTRACT: Histamine, a pivotal chemical within certain cells of the human body, is responsible for eliciting various allergic symptoms, such as sneezing and a runny nose. In cases of allergies, where the immune system misidentifies typically harmless substances, such as certain foods or dust, as harmful, an efficient histamine sensor becomes imperative. This research introduces a novel sensing platform by employing a material comprising hydrothermally synthesized WS_2 nanosheets and using this with a chitosan (CS) biopolymer on a screen-printed carbon electrode (SPE). Integrating WS_2 and CS components on the SPE via drop-casting synergistically enhances conductivity and various sensor properties. This novel hybrid material combines organic CS and inorganic WS_2 components applied for nonenzymatic histamine detection via differential pulse voltammetry. This study also included crystallite size determination and surface morphology assessment through characterization of the synthesized WS_2 nanosheets. On the surface of the SPE, WS_2 and CS were drop-casted. It is recommended that histamine be electrochemically measured on modified WS_2/CS/SPE electrodes. Histamine measurements were conducted within a linear coverage of 1−100 μM, with a limit of detection of 0.0844 μM and sensitivity of 1.44×10^{-4} mA/μM cm^2. The developed sensor exhibited notable levels of sensitivity, selectivity, stability, and repeatability, along with an extended linear range. The sensing technique was consequently employed to detect the histamine levels in packed food items like fermented food samples (cheese, tomato sauce, tomato ketchup, and soy sauce) at room temperature (25 °C). The findings recommend the utilization of electrochemical sensing on modified WS_2/CS/SPE electrodes for accurate histamine detection.

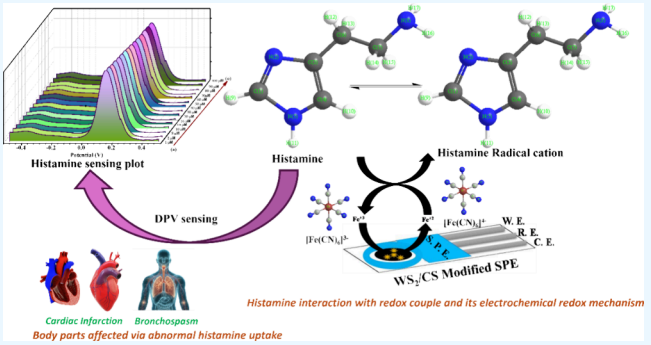

1. INTRODUCTION

Food readily gets contaminated, and conserving the freshness of food is of prime responsibility equally for consumers as well as the food industry, as inappropriate packing execution is capable of stimulating the maturation of microorganisms as well as bacteria, emerging food deterioration via free amino acid decarboxylation by using bacterial enzymes, and directing the formation of biogenic amines (BAs).[1,2] Food safety has transformed into a pivotal concern that needs to be addressed. Histamine is associated with a category of compounds recognized as biogenic amines. Histamine (2-(1*H*-imidazol-4-yl) ethanamine)[3] is produced by the decarboxylation of histidine,[4] which is activated via the enzyme L-histidine decarboxylase.[5−7] It is a vasoactive aquaphilic and biogenic amine (BA) that causes allergies[8] and/or human body intoxications, and also it may deteriorate the freshness of food.[7] Histamine levels indicate the freshness and quality of foods and beverages. Determining histamine levels in food and beverages is crucial due to its potentially harmful effects on humans. For instance, histamine detection is particularly interesting because of its implications in biomedical as well as in food safety applications, especially in monitoring histamine levels in biological samples including various fish products, packed food items like fermented foods, vinegar,[9,10] alcoholic beverages, and processed meat.[11] The primary source of histamine in food is histidine decarboxylation, which is aided by endogenous decarboxylases or microbial activity during food spoiling. Consuming foods with high histamine concentrations results in histamine poisoning.[8] Such poisoning causes symptoms such as headache, nasal discharge, bronchospasm, cardiac infarction, hypotension, and edema.[12] The United States Food and Drug Administration (USFDA) regulates the maximal acceptable quantity of histamine in fish and seafood stuff at 50 ppm, and the toxic level for human beings is 500 ppm.[13] These (BAs) are organic bases having low molar mass whichever particularly exist in surviving beings and consistently retain vital physiological activity.[14,15] The minor extent of BAs is frequently biosynthesized in flora as well as animalia kingdoms. Enormous

Received: November 16, 2024
Revised: December 24, 2024
Accepted: December 27, 2024
Published: January 14, 2025

quantities of it exist in fermented and deteriorated foods (fermented sausage, cheeses, vegetables, fish commodities, and liquor) as a consequence of microorganism amino acid decarboxylation.[16] Even though a modest extent of BAs is vital for living beings, BAs lead to foodborne illness at high concentrations.[17] Histamine is a uniformly existing BA as it is identified in various fruits, green vegetables, cheese, fish, beer, and red wine[8] at a quite small concentration. At the same time, when food is damaged, the quantity increases to a harmful range to an extent of 500 mg kg^{-1} of product, leading to foodborne illness.[8] The histamine content is also a prominent marker of food freshness, as well as quality. Histamine is feasibly developed during the manufacturing, packing, or transference of protein-rich foods employing changes in temperature or bacterial enzymatic decarboxylation of histidine.[18] Most of the physicochemical reactions occur in foodstuff during storage, and the reactions are lead via distinct agents like packaging procedures, moisture, light, heat, etc. Besides all these, adulterated foods are potent to transform the food content, which also leads to health constraints.[18] Fresh fish hold particularly low levels of histamine, despite the fact that spoiled fish have increased histamine levels. Hence, the histamine level is recommended as a natural freshness indicator of fish.[19] The US Food and Drug Administration (FDA) proposed that a standard limit for histamine for edible fish is 50 mg kg^{-1}, while the standard limit set by the European Union (EU) is 100−200 mg kg^{-1}, and fish having histamine levels more than those are proscribed from being traded for consumption of human.[20] For the food sector as well as food safety, detection of histamine is very crucial. Itching, sneezing, and gastrointestinal issues as well as potentially fatal conditions like anaphylactic shock are among the main symptoms of an allergic reaction.[21] The World Health Organization (WHO) listed that during the period from 2000 to 2020 one in 10 people was troubled with food poisoning. As stated by the WHO, around 420,000 human beings lose their lives annually due to foodborne illnesses, leading to an annual global expenditure of almost $100 billion on medication. This cost is expected to rise significantly due to the population explosion.[22] Food safety has evolved into a serious concern that needs to be suitably managed, as these are quickly contaminated.[23,24] Fish is recommended by nutrition experts as it is preciously little in fat, abundant in protein as well as omega-3 fatty acids, together with vitamins like D and B_2, and also more abundant in minerals including potassium, magnesium, iron, zinc, and iodine. Furthermore, the consumption of fish distributes varied goodness to the human body.[25] Decarboxylation in fish muscles results in BAs generally; histamine is widely studied. A higher extent of histamine existing in the bloodstream can lead to histamine poisoning, a food toxicity with symptoms ranging from mild to life-threatening.[26] Histamine analysis in foods is performed via various techniques, namely, thin-layer chromatography, capillary electrophoresis,[18] gas chromatography,[27,28] fluorometry,[29,30] and high-performance liquid chromatography (HPLC).[31,32] However, these approaches are extremely sophisticated as well as expensive and require a long analysis time and complex sample preparation procedures, whereas electrochemical biosensors are interesting substitutes for all of the above traditional techniques.[33,34] Subsequently, electrochemical biosensors are emerging as an economical,[35] accessible, instantaneous action with high selectivity as well as reliability[36] for histamine detection.

Screen-printed electrodes (SPEs) have been utilized to measure numerous compounds as a modest, disposable, nonhazardous, and low-cost substitute[37−39] over traditional solid electrodes. Histamine is essential for neuromodulation and the living immune response.[40] We investigated the mechanism of histamine reaction on SPEs and employed that evidence to develop improved fast-scan methods for histamine detection. Differential pulse voltammetry (DPV), being the most delicate electrochemical sensing[41] technique, has obtained much consideration lately. In this case, histamine is determined electrochemically using the DPV approach. This was accomplished through electrode modification with a composite material containing WS_2/chitosan. The electrode fabrication method was prepared, and the histamine detection parameters were optimized. Owing to its distinctive attributes, WS_2, a two-dimensional transition metal dichalcogenide (TMD), is noticeably important in electrochemical sensing as it possesses a large surface area,[42] thereby providing multiple interaction sites for analytes. WS_2 is a semiconductor that offers tunable conductivity through layer count or defect introduction, making it flexible for sensors. Sulfur vacancies enhance catalytic properties and redox reactions. Its adjustable band gap enables versatile electronic and optoelectronic applications. With its chemical stability and resistance to oxidation, WS_2-based sensors provide a long-lasting performance and rapid response times along with low detection limits, accomplishing appropriate, continuous, and reliable sensing in various environmental conditions. WS_2 has a layered structure that is stacked together via weak van der Waals forces,[43] and the sulfur atoms in the structure help to protect the tungsten atoms from oxidation. This inherent oxidation resistance is crucial for maintaining material sensing performance over time, even in the presence of oxygen or other oxidizing agents. WS_2 offers fast electron transfer properties,[44] which can lead to rapid response times for electrochemical sensors, making them suitable for real-time monitoring.[45] WS_2 has a direct band gap after exfoliation in a single layer, which makes it optically active. This property is crucial for applications in optoelectronics and photonics.[46] Tunable conductivity, achieved by controlling layers or introducing defects, allows for a sensor design with varying sensitivities. Its catalytic activity in redox reactions, including water splitting, enhances its electrochemical capabilities. WS_2 nanosheets impart a high surface area[38,44] for enhancing active sites in electrochemical sensors. Engineered with a high surface area along with rapid electron transfer properties, WS_2-based sensors offer a rapid response time for real-time monitoring. Functionalization with different molecules or nanoparticles enhances selectivity, and WS_2-based sensors demonstrate the potential for low detection limits in trace-level analysis. Incorporation into various sensor configurations, such as screen-printed electrodes, further expands its application versatility.

Advancement in histamine electrochemical detection requires improvement in sensitivity as well as selectivity to accurately detect minuscule amounts in biological samples along with other analytes such as ascorbic acid, glutamic acid, vitamin B_{12}, glucose, urea, etc. Here, we are demonstrating the histamine levels in diverse packed food items as well as in fermented food samples (cheese, tomato sauce, tomato ketchup, and soy sauce) at room temperature (25 °C). High sensitivity is required for detecting low histamine levels, whereas for separating histamine from other interfering substances, excellent selectivity is required. Furthermore, it was observed that the existence of a variety of amines as interfering agents was unable to create some notable interfering influence in the assessment of histamine.

https://doi.org/10.1021/acsomega.4c10419
ACS Omega 2025, 10, 3153−3164

Scheme 1. Outline of the Synthesis of the WS_2 Material, Utilized for Modifying SPE Electrodes, Which Are Then Applied in Histamine Sensing

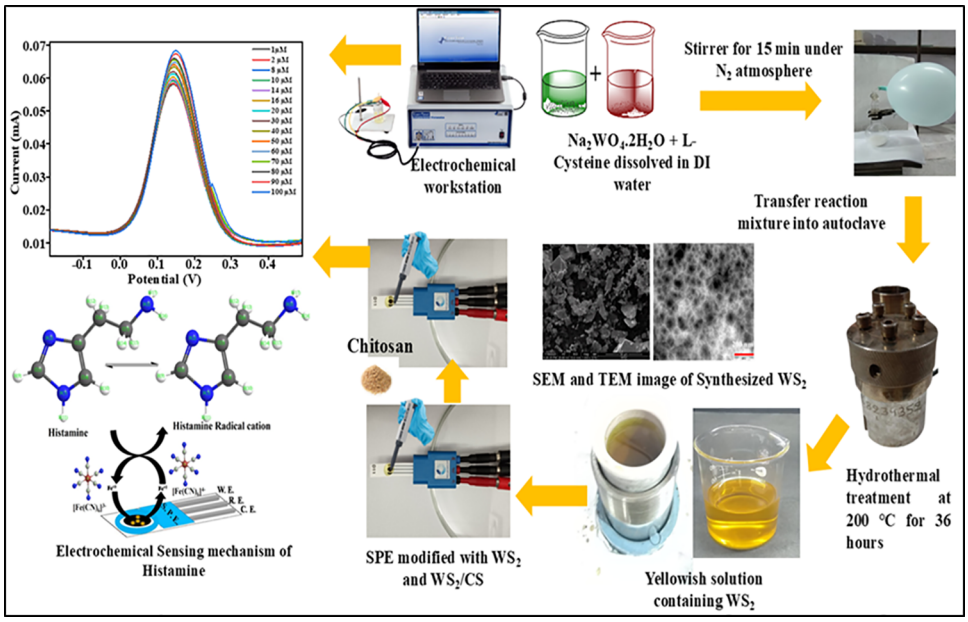

2. EXPERIMENTAL SECTION

2.1. Materials and Methods. For the WS_2 NP synthesis, the subsequent chemical reagents utilized are $Na_2WO_4{\cdot}2H_2O$, L-cysteine, and HCl. Additionally, $K_4[Fe(CN)_6]{\cdot}3H_2O$, $K_3[Fe(CN)_6]$, $[Na_2HPO_4{\cdot}2H_2O]$ (99%), $[NaH_2PO_4{\cdot}2H_2O]$ (98–100.5%), and NaCl (99%) were procured from Merck Specialties Private Ltd., Mumbai, India, and were applied for the preparation of phosphate buffer saline (PBS) with a redox couple. Throughout the experiment, the solution was prepared in deionized (DI) water.

2.2. Synthesis of WS_2 Nanoparticles. $Na_2WO_4{\cdot}2H_2O$ (0.25 g) was solvated in 20 mL of DI. To bring the pH to 4.0, 0.1 M HCl solution was used. Then, in another beaker, 0.5 g of L-cysteine was solvated in 50 mL of DI. After mixing both the solutions thoroughly, they were evenly dispersed for 10 min. The resulting solution was then placed in an autoclave and subjected to heating in a muffle furnace at 200 °C for 36 h. Subsequently, the autoclave was allowed to cool naturally at room temperature; sequential filtration and washing with distilled water were performed, until a yellowish solution containing WS_2 was obtained. This solution was then used for subsequent structural and electrochemical analyses.

2.3. Preparation of Standard Stock Solution. Histamine was dissolved in Milli-Q water to produce a fresh histamine solution, which was then kept at 4 °C for further testing. Then, to create analytes of various concentrations, a 1 mM stock solution was made and diluted with Milli-Q water.

2.4. Drop-Casting of the WS_2 and CS on the SPE to Form the WS_2/CS/SPE-Modified Electrode. First, the SPE was modified by drop-casting WS_2 on it. This WS_2-modified SPE was further recast with chitosan (CS). Modifying a screen-printed electrode (SPE) with both WS_2 and CS simultaneously enhances its catalytic properties in contrast to the SPE modified with WS_2 alone. CS enhances stability through film formation, improves adhesion, and contributes to an increased conductivity. This exhibits biocompatibility,[47] making it suitable for biological applications,[48] while potential synergistic effects enhance WS_2 electrocatalytic properties. CS introduction of functional groups alters chemical interactions, and its unique properties enhance selectivity in detecting different analytes. The primary functional groups in CS that contribute to its increased adhesion properties include amino groups and hydroxyl groups.[49] Hydroxyl groups participate in hydrogen bonding, which enhances the adhesive properties of CS. The combination of amino and hydroxyl groups allows CS to interact with a variety of surfaces through different bonding mechanisms. The modified electrode is utilized in biological sensing, selectivity improvement, and overall electrocatalytic performance, which is represented in Scheme 1.

2.5. Sensing Mechanism of Histamine on WS_2/CS/SPE. When 2D nanosheets of tungsten disulfide (WS_2) and CS are used for histamine sensing, the interactions involved in the sensing process primarily revolve around the adsorption of histamine molecules onto the nanocomposite surface[50] and ensuing signal transduction, which is produced during the interactions that occur at the time of histamine sensing with WS_2/CS. Histamine molecules present around the adjacent domain adsorb onto the surface of the WS_2/CS/SPE electrode, and the adsorption process is typically driven by various chemical interactions, including electrostatic interactions. CS is a biopolymer that is derived from chitin and contains amino groups (NH_2) that form electrostatic interactions with histamine, which contains both acidic and basic functional groups. The CS also contains hydroxyl groups (OH) that form hydrogen bonds with histamine, which can form bonds both with hydrogen donors as well as acceptor groups.WS_2, which belongs to the family of 2D layered TMDs, and the π electrons in its layers interact with the π electrons of the histamine molecule, facilitating $\pi-\pi$ stacking interactions. This interaction between histamine and the WS_2/CS/SPE electrode is utilized for histamine sensing. Changes in the properties of the nanocomposite due to histamine adsorption were monitored, and these changes are correlated with histamine concentration. The current variations direct the histamine concentration and are also quantified for recognition. During electrochemical histamine sensing, variations in the electrical conductivity or

https://doi.org/10.1021/acsomega.4c10419
ACS Omega 2025, 10, 3153−3164

electrochemical properties of the WS_2/CS/SPE electrode occur due to histamine binding. A radical is formed due to a one-electron transfer from histamine's imidazole ring.[51,52]

2.6. Histamine Redox Reaction with a Mediator. During the histamine oxidation process, one electron from a lone pair of $-NH_2$ (N8) participates in the electrochemical reaction during DPV sensing and forms a histamine radical cation. The lone pair of electrons present on N of the imidazole ring (N2 and N5) is delocalized as well to maintain its resonance energy and is not involved in an electrochemical process. The electron released from histamine is accepted via $[Fe(CN)_6]^{3-}$ and forms $[Fe(CN)_6]^{4-}$, which is a redox mediator throughout the electrochemical study. The overall redox reaction is represented by combining the redox process of histamine and the redox couple reactions, as shown in Scheme 2.

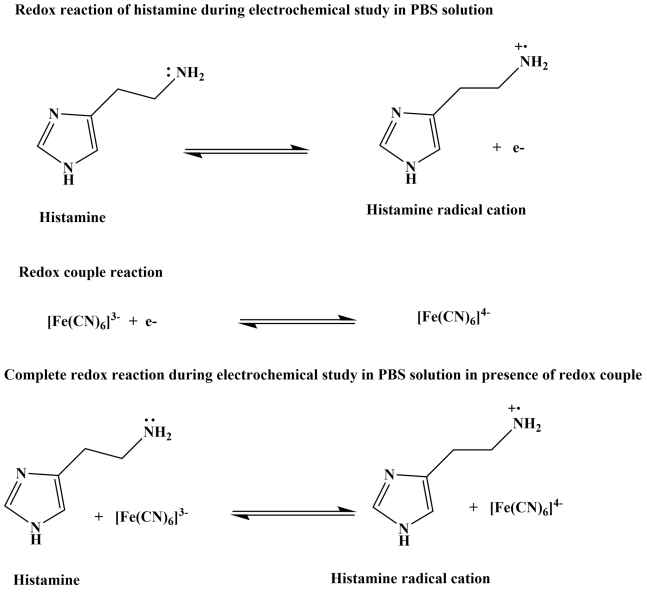

Scheme 2. Histamine Complete Redox Reaction with the Mediator during an Electrochemical Study in PBS Solution Containing Ferri/Ferrocyanide as a Redox Couple

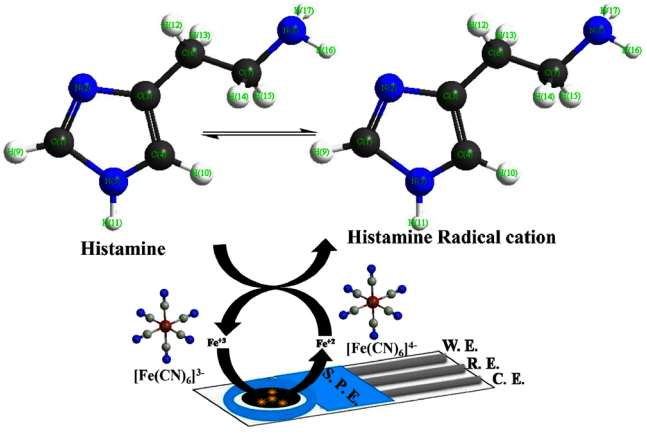

2.7. Characterization Techniques. For the study of the various structural and morphological characteristics, different characterization techniques were utilized. For example, Fourier transform infrared (FTIR) spectroscopy was proficiently performed via FTIR and ATR accessory (Jasco, Tokyo) apparatus; the spectra of the material were obtained, which mostly extend from 4000 to 400 cm^{-1}; moreover, the sample was prepared using KBr pellets. Along with IR spectroscopy, Raman spectroscopy (WI Tec Alpha Zoo Focus Innovations) was also used to characterize the structural features of the prepared material. Consequently, the measurement was recorded by utilizing a 633 nm laser as an excitation source to reveal the WS_2 Raman spectra. The material was characterized by a PAN Analytical EMPYREAN RAYONS-X diffractometer accompanied by Cu Kα X-ray radiation at a scanning step size of 0.013° having a wavelength of 0.154056 nm. Also, the 2θ values at which the spectra were recorded range from 10 to 80°. The yellowish solution containing WS_2 was drop-cast onto a glass slide, acting as a substrate to achieve a uniform layer, and consequently dried overnight in a vacuum oven before being subjected to p-XRD, XPS, and Raman analysis. The glass slide taken from Blue Star (micro cover glass) [Polar Industrial Corporation, Mumbai, India] is 18 × 18 mm^2, and the thickness is 0.13−0.16 mm made of a glass material. The X-ray photoelectron spectroscopy (XPS) estimation was administered using a PHI 5000 Versa Probe III Photoelectron Spectrometer that includes an Al Kα monochromatic X-ray source with a photon energy of 1486.6 eV. The instrument allows for the adjustment of the Al Kα X-ray spot size, ranging from 10 to 200 μm, and scanning XPS with dimensions up to 1.4 mm. Using a transmission electron microscope (TEM), a Tecnai G^2 20 Twin, operating at 200 kV, high-resolution TEM (HR-TEM) and selected-area electron diffraction pattern (SAED) pictures were captured. The prepared yellowish-colored solution of WS_2 was diluted further by adding DI water, which was then drop-cast on the TEM grid formed by Cu and carbon having 300 mesh followed by drying the sample, and finally, its TEM analysis was performed. Scanning electron microscope (SEM) analysis was executed for the morphological studies of the synthesized material utilizing a Carl Zeiss SEM, operated at a voltage of 20 kV. Lanthanum hexaboride (LaB_6) is a cathode employed for the creation of enormously energetic electrons, and these are utilized to execute surface information on the materials. For SEM analysis, the solution was drop-cast on the SPE; subsequently, the sample was dried and its SEM spectra were recorded. The energy-dispersive X-ray (EDX) spectroscope affixed with a Tecnai G^2 20 Twin microscope was utilized for compositional analysis and elemental mapping.

3. RESULTS AND DISCUSSION

3.1. X-ray Diffraction Analysis. The samples were drop-cast onto an 18 × 18 mm^2 glass slide (0.13−0.16 mm-thick) for uniformity and then dried overnight in a vacuum oven before p-XRD analysis. We have included the XRD spectrum of the glass slide in the Supporting Information to display that the glass slide does not show any interference in the p-XRD spectrum of the WS_2 nanosheets. The p-XRD image of the glass slide is shown in Figure S1. The XRD intricateness of WS_2 nanosheets is illustrated in Figure 1a. The pattern illustrates the crystalline behavior of synthesized WS_2. The crystallite size of WS_2 nanosheets is calculated by the Scherrer equation discussed and utilized for the calculation of average crystallite size (eq 1).[53] The WS_2 NPs showed peak positions at 2θ values of 15.55, 28.85, 31.7, 45.31, and 47.71°. The corresponding Miller indices are, respectively, (003), (006), (101), (009), and (107), which resemble perfectly with JCPDS card no. #84-1399,[54] confirming the rhombohedral crystal structure and rhomb-centered lattice unit. Because of the hexagonal crystal phases present in WS_2, it shows some small Bragg reflections in the XRD spectra resembling the planes (100), (102), and (106) corresponding

https://doi.org/10.1021/acsomega.4c10419
ACS Omega 2025, 10, 3153−3164

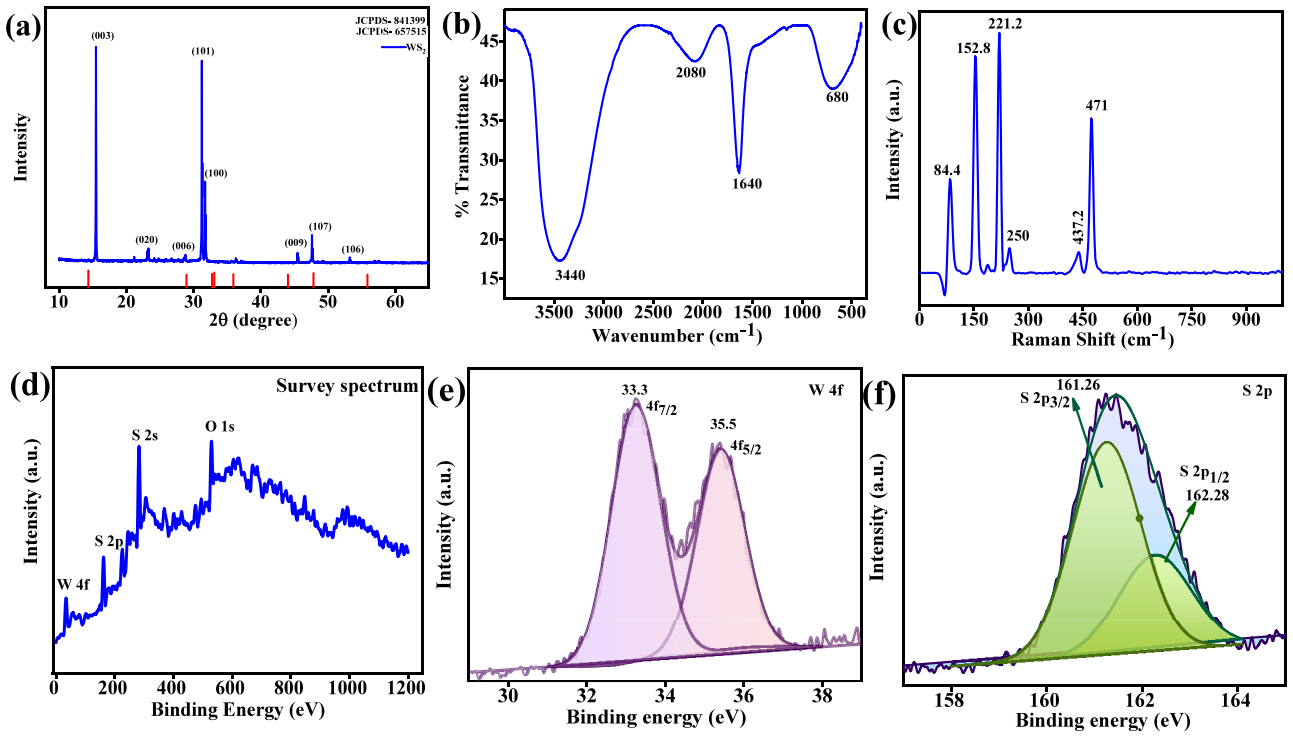

Figure 1. (a) XRD plot, (b) FTIR spectrum, and (c) Raman spectrum of prepared WS_2. (d) Survey spectrum of the $WS_2$and (e) deconvoluted W 4f spectrum and (f) deconvoluted S 2p spectrum of the prepared WS_2.

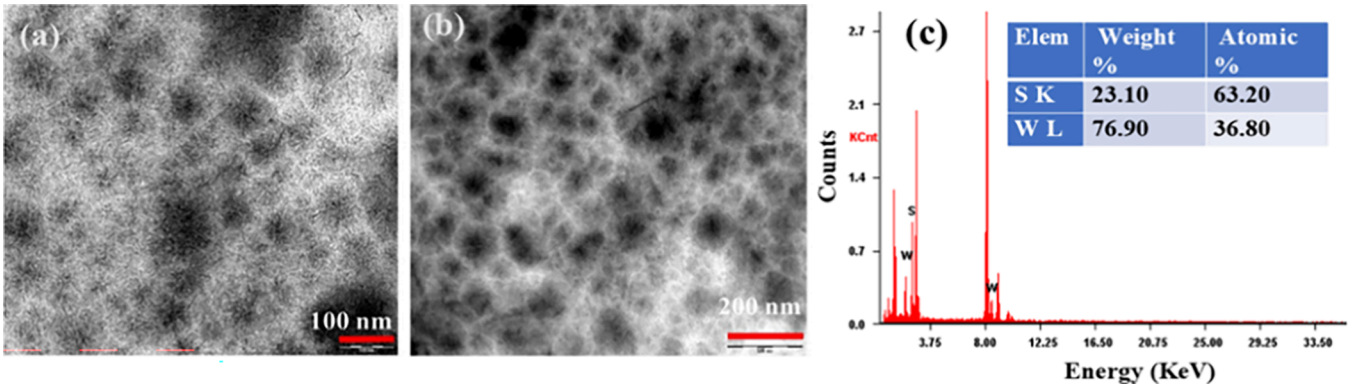

Figure 2. (a, b) TEM images of the synthesized WS_2 nanosheet at different magnifications. (c) EDAX spectrum of the synthesized WS_2 nanosheet and an inset table displaying the weight and atomic percentages of the WS_2 nanosheet.

to 2θ values of 31.86, 36.3, and 53.4°, respectively, matched with JCPDS card no. [657515]. Some traces of WO_3 are identified in the XRD and XPS spectra. By comparison of the peak intensity and position with the JCPDS standard value, the phase of the nanoparticles was verified. The average crystallite size of the nanoparticles was found to be 94 nm, and the crystallite size was measured using a very intense Braggs peak at 15.55°, shown in eq 1

$$D = K\lambda/\beta \cos\theta \quad (1)$$

in which D is the average crystallite size, K is the Scherrer constant (which is 0.9), λ is the wavelength of X-rays (1.54056 Å), β is the full-width at half maxima in radian, and θ is the Bragg's angle in degrees.

3.2. FTIR Analysis. The synthesized WS_2 NPs show characteristic FTIR bands at 3440, 2080, 1640, and 680 cm^{-1}. The frequency observed at 680 cm^{-1} was assigned to the W−S stretching vibration band,[55] which is shown in Figure 1b. The band observed at 3440 cm^{-1} accounted for the O−H stretching of the associated water molecule, and the band obtained at 1640 cm^{-1} was affiliated with the C=C stretching.[54]

3.3. Raman Analysis. The prepared WS_2 nanosheets exhibit characteristic peaks at 84.4, 152.8, 212.2, 250, 437.2, and 471 cm^{-1} in the Raman analysis. The band obtained at 437.2 cm^{-1} in the Raman spectra of WS_2 represents the out-of-plane vibrational mode with A_{1g} symmetry,[51,56,57] which is shown in Figure 1c.

3.4. X-ray Photoelectron Spectroscopy (XPS) Analysis. The XPS survey of the WS_2 is shown in Figure 1d, which presents the survey plot consistent with the WS_2 nanosheet, distinctly showing the peaks related to W and S. The two notable peaks attributed to W^{4+} at 33.3 and 35.5 eV are assigned to the W $4f_{7/2}$ and W $4f_{5/2}$ orbitals, respectively,[55,56] as shown in Figure 1e. The S $2p_{3/2}$ and S $2p_{1/2}$ orbitals of the bivalent sulfide ion are represented by the two broad peaks in Figure 1f, which are seen at 161.26 and 162.28 eV.[58] These peak energy locations suggest

https://doi.org/10.1021/acsomega.4c10419
ACS Omega 2025, 10, 3153−3164

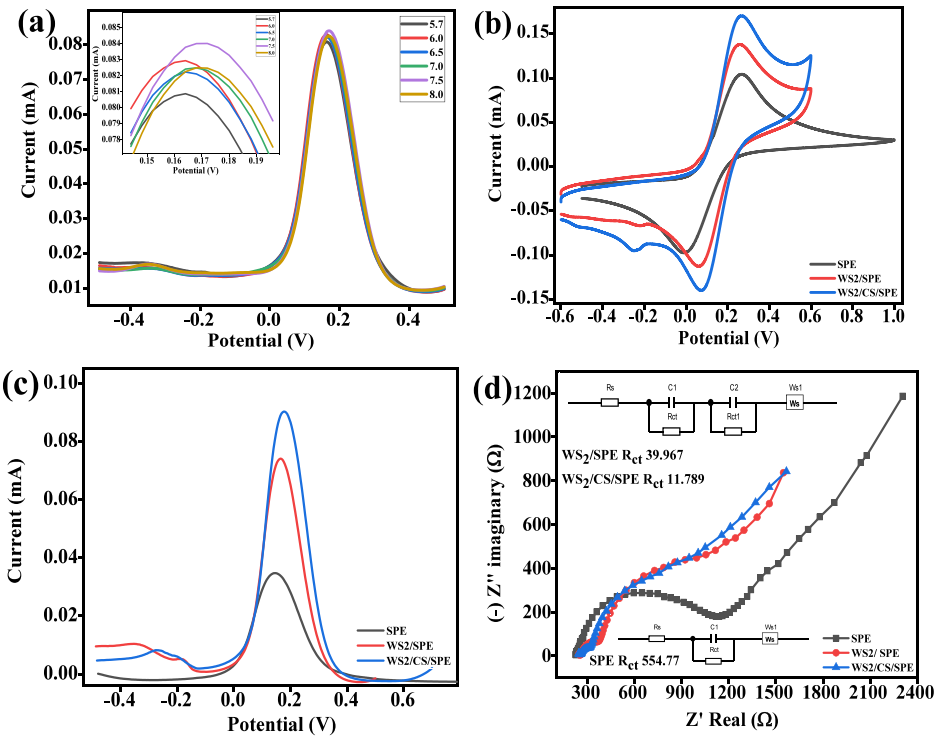

Figure 3. (a) DPV voltammograms of WS_2/CS/SPE at different pH (pH optimization plot) with a zoomed inset of pH optimization. (b) Cyclic voltammograms, (c) DPV voltammograms, and (d) EIS plot of the different electrodes (bare SPE, WS_2-modified SPE, and WS_2/CS-modified SPE) in PBS.

valences of +4 and −2 that correspond to W and S, which aligned with the preceding findings showing the formation of the WS_2 phase. Figure S5 exhibits the XPS spectra before and after the charging effect. Table S8 presents the S 2p XPS spectrum (a and c) and W 4f XPS spectrum (b and d) and spectrum χ^2 constraint values during the fit procedure before the charging effect.

3.5. Transmission Electron Microscopy (TEM). TEM images show individual irregular shapes and few-layer sheets with diameters of up to the nm scale, which is shown in Figure 2a,b. The few-layer sheet-like structure is further validated by the SEM image of the synthesized WS_2 nanosheets. Figure 2c depicts the atomic and elemental composition of the WS_2 nanosheet, which is described using energy-dispersive analysis of X-rays (EDAX). The X-rays that are created when the electron beam interacts with the material are detected by EDAX. The production of the WS_2 nanosheet has been confirmed by the experimentally measured values of the element W and S atomic compositions, which are determined to be 36.80 and 63.20%, respectively, and their weight compositions are 76.9 and 23.1%, respectively.

3.6. Scanning Electron Microscopy (SEM). The SEM images of the bare SPE and the SPE drop-cast with the synthesized WS_2 nanosheet were recorded, confirming the nanosheet-like shape of WS_2. These nanosheets of WS_2 provide a large surface area for electrochemical detection of histamine. The corresponding figures are given in the Supporting Information (Figure S2).

3.7. Electrochemical Study. All the oxidation−reduction aspect of the WS_2/CS/SPE electrode was evaluated by dipping it in a solution comprising a 50 mM PBS (consisting of 0.9% NaCl) solution of pH 6.0 and a redox couple ferri/ferrocyanide having 5 mM concentration at a scan rate of 50 mV s^{-1}, fabricated by drop-casting the WS_2/CS composite on the SPE. Since the density of solution changes at higher concentrations, such as 5−10 mM, disrupting the double layer that possibly decreases the significance, the concentration of the ferri/ferrocyanide redox probe has been chosen to be between 0.5 and 5 mM to have a suggestively raised signal-to-background and signal-to-noise ratio. The potential parameters, ranging from −0.6 to 0.6 V, were reported for respective electrochemical studies.

3.7.1. pH Optimization. As explained in the section on electrochemical analysis, the electrode's electrochemical properties were investigated by adjusting the pH values between 5.7 and 8 in PBS using the DPV technique. Figure 3a exhibits the corresponding voltammetric responses. At pH 5.7 and 6, the oxidation/anodic peak current rose, peaking at 0.084 mA at pH 7.5. At pH 6.5, 7, and 8, a further decrease in the current was noted. Changes in the buffer's pH are accountable for the increase in current; the current response is greatest at pH 7.5. Therefore, pH 7.5 was chosen for further electrochemical research. Since pH impacts the redox potential, species accessibility, and proton−electron transport, it must be tuned to enhance electrochemical kinetics and electrode stability. The WS_2/CS nanocomposite in PBS buffer in this investigation has a pH of 7.5, which represents maximum current adaptability and optimal charge transfer.[59]

3.7.2. CV, DPV, and EIS Studies of the Bare and Modified SPEs. As illustrated in Figure 3b, the bare SPE electrode exhibits an apparent oxidation current at 0.106 mA. After drop-casting WS_2 on the bare SPE, a delicate increment in the oxidation current was noted (i.e., 0.140 mA), which was further increased upon drop-casting the WS_2/CS nanocomposite on the SPE (0.173 mA). The redox performance of the bare SPE, WS_2/SPE, and WS_2/CS/SPE toward 5 mM ferri/ferrocyanide in 0.9%

https://doi.org/10.1021/acsomega.4c10419
ACS Omega 2025, 10, 3153−3164

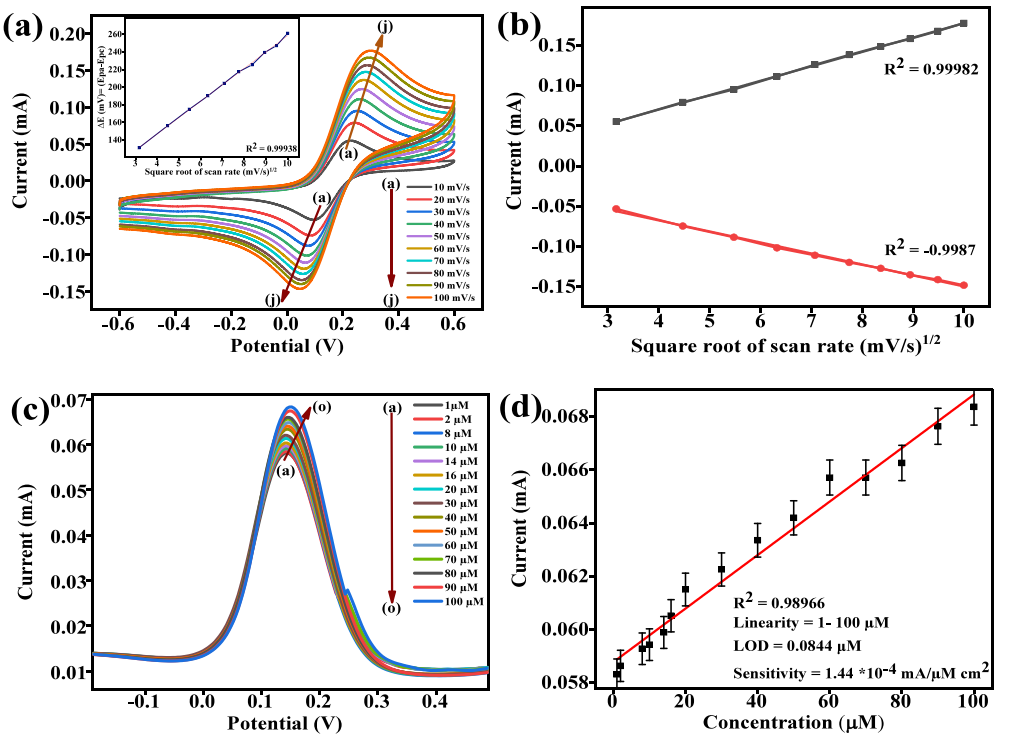

Figure 4. (a) Scan rate plot of the WS_2/CS/SPE at different scanning rates with the inset of the calibration plot of the ΔE vs square root of scan rate. (b) Calibration scheme of the current values vs square root of scan rate. (c) DPV curves of WS_2/CS/SPE with different concentrations of histamine (1−100 μM). (d) Calibration scheme of DPV current vs different concentrations of histamine in PBS.

NaCl was assessed via cyclic voltammetry (CV) at a scan rate of 50 mV/s. WS_2/CS/SPE has distinct redox peaks with the highest peak existing at the lowest potential difference. The surface-active area was resolved via the Randles−Sevcik equation (eq 2)

$$\mathrm{Ip} = 2.69 \times 10^5 n^{3/2} \mathrm{AD}^{1/2} \mathrm{Cv}^{1/2} \quad (2)$$

Here, Ip is the peak current (amp), n is the extent of electrons transported in the electrocatalytic redox reaction, A is the effective electrode area (cm^2), D is the diffusion coefficient of ferri/ferrocyanide (7.6×10^{-6} cm^2 s^{-1}), and C is the ferri/ferrocyanide concentration (5×10^{-6} mol cm^{-3}). The bare electrode had a surface area of 0.128 cm^2. The area of WS_2/SPE was calculated to be 0.168 cm^2 and that of WS_2/CS/SPE to be 0.208 cm^2. Based on these outcomes, we conclude that the composite-modified electrode has a highly surface-active region for electrochemical sensing.

The CV study of the electrode was further validated by the DPV study of the electrode, as displayed in Figure 3c. The bare SPE electrode illustrates a clearly defined oxidation current at 0.036 mA. An increase in oxidation current, measured at 0.075 mA, was seen after the WS_2 was drop-cast on the bare SPE. This current increases to 0.091 mA with the drop-casting of the CS on modified WS_2/SPE to form WS_2/CS/SPE. Histamine oxidation is facilitated by increased electron transport promoted by WS_2/CS. The EIS approach was employed to examine the electrochemical properties of the bare SPE, WS_2/SPE, and WS_2/CS/SPE. Figure 3d shows the Nyquist plot of the bare SPE, WS_2/SPE, and WS_2/CS/SPE, in the presence of 0.9% NaCl solution consisting of 5 mM ferri/ferrocyanide. The semicircular diameter indicates the resistance level of the electrode surface. The EIS plot estimates R_{ct} values of 554.77, 39.967, and 11.789 Ω for the bare SPE, WS_2/SPE, and WS_2/CS/SPE, respectively.

The subsequent equation is known to acquire the charge transfer rate constant (K_s) of diverse bare and modified electrodes (eq 3)3

$$K_s = \mathrm{RT}/n^2F^2\mathrm{AR}_{ct}C \quad (3)$$

where K_s is the charge transfer rate constant, n is the number of electrons, R is the universal gas constant (8.314 J K^{-1} mol^{-1}), T is the room temperature (27 °C), F is the Faraday constant (96500 C mol^{-1}), A is the surface area of the electrode (cm^2), C is the ferri/ferrocyanide concentration (5×10^{-6} mol cm^{-3}), and R_{ct} is the resistance for charge transfer. The charge transfer rate constants for the bare SPE, WS_2/SPE, and WS_2/CS/SPE are 7.54×10^{-4}, 7.98×10^{-3}, and 2.18×10^{-2} cm s^{-1}, respectively. The WS_2/CS/SPE exhibits the lowest resistance (R_{ct}) in comparison to the bare SPE and WS_2/SPE, and a lower R_{ct} value of 11.789 Ω verifies the faster electron transfer mechanism on the WS_2/CS/SPE electrode. In electron transfer reactions, a higher K_s implies faster electron transfer, while a lower K_s implies slower transfer. Hence, the reaction with higher K_s is faster and more efficient in electron transfer. Thus, our modified electrode has the highest electron transfer rate, which is suitable for electrochemical sensing applications.

3.7.3. Scan Rate and Kinetics Analysis. The scan rate study is carried out extending from 10 to 100 mV s^{-1}, which is presented in Figure 4a (the bare SPE scan rate plot is accessible as Figure S6). The interfacial kinetics of the WS_2/CS/SPE were identified from the scan rate study owing to the altering scan rate. As shown in Figure 4b, it has been found that the scan rate fluctuates linearly with the anodic/oxidation (Ipa) and cathodic/reduction (Ipc) current peak extents. A linear plot between Ip vs $v^{1/2}$ was obtained, which gives information about

https://doi.org/10.1021/acsomega.4c10419
ACS Omega 2025, 10, 3153−3164

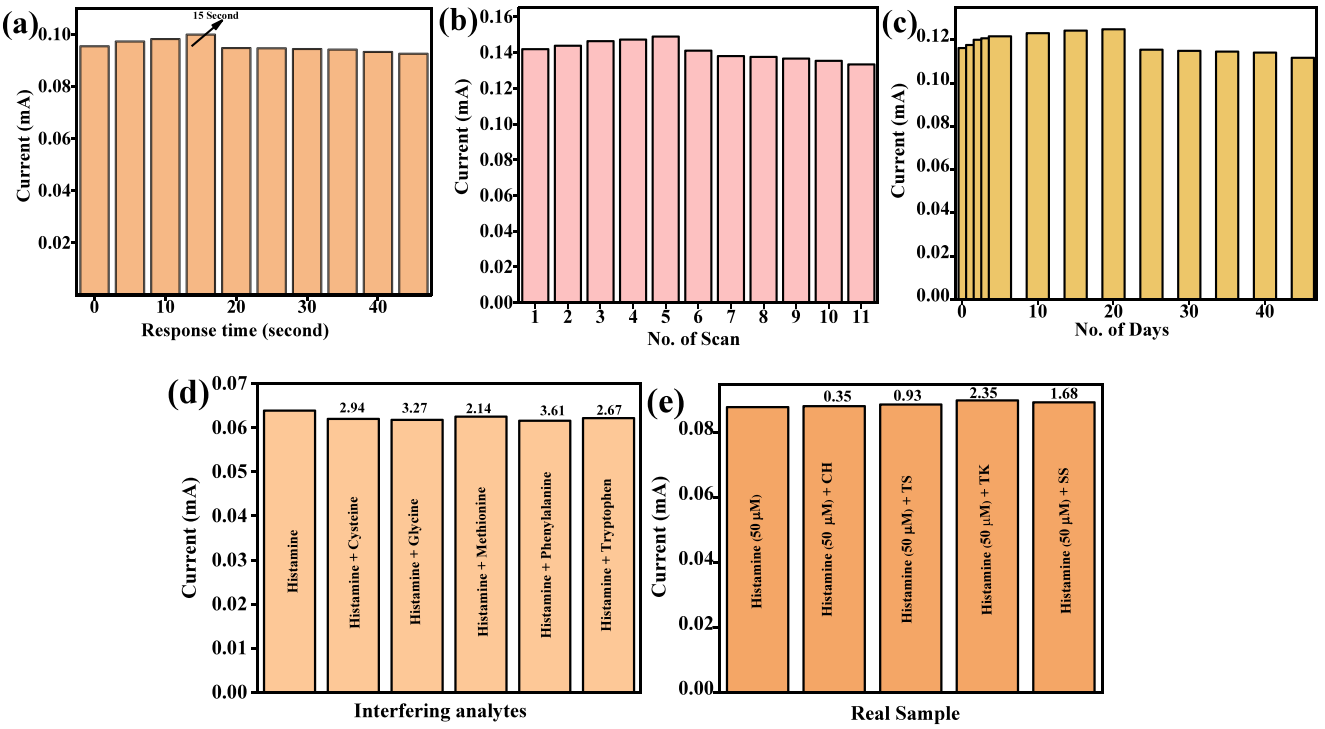

Figure 5. (a) Response time, (b) reusability, and (c) stability analysis of the prepared WS_2/CS/SPE electrode. (d) Bar graph of the interference study of histamine and (e) bar graph of real sample analysis of histamine on the WS_2/CS/SPE electrode in 50 mM PBS (consists of 0.9% NaCl) solution of pH 7.5 comprising 5 mM ferri-/ferrocyanide as a redox couple at a scan rate of 50 mV s^{-1}.

the electron transfer by surface adsorption, i.e., an adsorption-controlled process.[60] From the reversible limit $E_{pa} - E_{pc}$ (ΔE) = 57 mV, these chemical systems move over a whole zone. The peak-to-peak separation (ΔE) is a key parameter for evaluating the electrochemical properties of sensing materials. While peak separations continue to extend from reversible to irreversible (57−250 mV), they fall into a quasi-reversible range of 131 to 261 mV, which is measured in the inset of Figure 4a (description are provided in Table S1a,b).[61,62]

The Lavrion model[63] is employed to evaluate the rate constant for charge transfer (K_s) of the electrochemical reaction (s^{-1}) shown in eqs 4 and 5

$$m = (\mathrm{RT}/F)(K_s/n\upsilon) \tag{4}$$

$$K_s = mnF\upsilon/\mathrm{RT} \tag{5}$$

Here, "υ" is the scan rate (50 mV/s), m is a separation within a peak (calculating the potential difference ($\Delta E_p = E_{pc} - E_{pa}$) at 50 mV/s), and "$n$", "$F$", "$R$", and "$T$" have their usual meaning. By employing the aforementioned values of standards, the K_s assessed for the WS_2/CS/SPE electrode is 0.395 s^{-1}. The surface concentration of the WS_2/CS/SPE is conceivably estimated by implementing the Brown−Anson model,[64−67] which is as stated in the sequential equation (eq 6)

$$\gamma = \mathrm{Ip} \times 4\mathrm{RT}/n^2F^2A\upsilon \tag{6}$$

Here, "γ" is the surface concentration of the WS_2/CS/SPE electrode (mol cm^{-2}), "A" is the modified electrode's surface area (0.208 cm^2), and "F", "R", "υ", "n", and "T" are mentioned earlier. The surface concentration of the WS_2/CS/SPE electrode was determined to be 1.78×10^{-8} mol cm^{-2}.

The Randels−Sevcik equation[60] (eq 7) was used to estimate the diffusion coefficient (D) of the WS_2/CS/SPE electrode

$$D = \left(\frac{\text{slope}}{0.4463nFAC^0}\right)^2 \frac{RT}{nF} \tag{7}$$

Here, "D" is the coefficient of diffusion (cm^2 s^{-1}), "A" is the modified electrode surface area (0.208 cm^2), "n", "F", "R", and "υ" have their usual meaning, "T" generally is the room temperature (300 K), and "C^0" is the analyte concentration (concentration of the ferri-/ferrocyanide redox probe, which is 5×10^{-6} mol cm^{-3}). The "D" value was obtained to be 1.03×10^{-2} cm^2 s^{-1}.

3.7.4. DPV Sensing of Histamine on the WS_2/CS/SPE Electrode. The developed procedure has been shown to work with histamine. Under ideal conditions, DPV tests were taken at different concentrations of histamine solutions to estimate the functionality of the sensor. There is a comparable linear behavior among the DPV current estimates along with the histamine concentrations as the histamine concentration increased, which is displayed in Figure 4c,d with a linear regression coefficient (R^2) 0.98966. Histamine detection within linear ranges of 1−100 μM was established by this proposed approach. The electrochemical reaction at low histamine concentrations is displayed in the region of linear association at histamine concentrations extending up to 1−100 μM. At lower concentrations of histamine (20 μM), the signal-to-noise ratio results in ∼3:1. To assess this, the amplitude of the baseline noise was approximated with the amplitude of transposition in the signal from baseline, subsequently adding 20 μM histamine to the solution.

The limit of detection (LoD) and sensitivity are 0.0844 μM and 1.44×10^{-4} mA/μM cm^2, respectively. The suggested approach demonstrated improved sensitivity (lower detection limits). The LoD is evaluated via eq 8

$$\mathrm{LoD} = 3\mathrm{SD}/\mathrm{slope} \tag{8}$$

https://doi.org/10.1021/acsomega.4c10419
ACS Omega 2025, 10, 3153−3164

Table 1. Comparative Study of Fabricated WS_2/CS/SPE Electrode Histamine Sensor Parameters Compared with Those Reported Previously[a]

method	modified electrode	detection range (μM)	LoD (μM)	sensitivity	reference
CV	DAO-CS-AuNPs/PB/MWCNTs/SPCE	2.5−125.0 μM and 125.0−400.0 μM	1.81 μM		68
CV	GCE/CeO_2-PANI/DAO	450−1050 μM	48.7 μM	724.94 μA/mM cm^2	69
DPV	Nafion-MWCNTs/GCE	0.5−10 μM, 20−200 μM	0.39 μM		52
DPV	SWCNT/CPE	4.5−720 μM	1.26 μM		11
DPV	MIP/L-cysteine/AuNPs/GCE	1−107 μM	0.6 μM		5
DPV	WS_2/CS/SPE	1−100 μM	0.0844 μM	1.44×10^{-4} mA/μM cm^2	this work

[a]Where DAO-CS-AuNPs/PB/MWCNTs/SPCE stands for diamine oxidase (DAO) chitosan-gold nanoparticles (CS-AuNPs)/Prussian blue (PB)/multiwalled carbon nanotubes/screen-printed carbon electrode,[68] GCE/CeO_2-PANI/DAO stands for glassy carbon working electrode/CeO_2-polyaniline/diamine oxidase,[69] Nafion-MWCNTs/GCE stands for Nafion-multiwalled carbon nanotubes/glassy carbon electrode,[52] CPE means carbon paste electrode, and MIP/L-cysteine/AuNPs/GCE refers to molecular imprinted polymer/L-cysteine/gold nanoparticles/glassy carbon electrode.[5]

where SD is the standard deviation of the sensing response and also takes the slope of the calibration curve.

3.7.5. Response Time Study of Histamine on the WS_2/CS/SPE Electrode. The CV approach is used to estimate the response time. To determine the response time, we introduce an analyte to the PBS and begin measuring right away, within 0 and 45 s. The scan rate used in the response time investigation is 50 mV/s. The analyte's interaction with electroactive species is illustrated by a bar graph of response time versus current (mA) shown in Figure 5a [matching CV curve in Figure S3a]. At 15 s, we found maximum response in terms of current, and after that, the current is almost stable up to 45 s (particularly available in Table S2). From here, we affirm that at 15 s, maximal interaction occurs, and there is a quick response observed during electrochemical sensing of histamine.

3.7.6. Reusability and Stability of Histamine on the WS_2/CS/SPE Electrode. Reusability and stability of the sensor are significant for studying the sensing behavior. During reusability and stability analysis, we took data from CV at a 50 mV/s scan rate. From the reusability bar graph, which is shown in Figure 5b [corresponding CV curve in Figure S3b; details for reusability are available in Table S3], we found that the sensor is reusable up to 11 scans. The stability study was checked up to 60 days, but we observed that after 45 days of study, there was a large decrease in current. The electrode was stable from 25 to 45 days, which is shown in Figure 5c [corresponding CV curve in Figure S3c; details for stability are available in Table S4]. Table 1 presents the comparative study of fabricated WS_2/CS/SPE electrode histamine sensor parameters with those reported previously.

3.7.7. Interference Study of Histamine on the WS_2/CS/SPE Electrode. To check the selectivity of the fabricated WS_2/CS/SPE electrode to facilitate and administer the effects of some analytes that are also instant in blood including histamine, 50 μM histamine in PBS pH 7.5 with the accretion of distinct interfering agents was utilized, denoted in the bar graph of Figure 5d [corresponding CV curve in Figure S4a]. For the interference study, we employed diverse amines as interfering analytes like cysteine (20 μM), glycine (20 μM), methionine (20 μM), phenylalanine (20 μM), and tryptophan (20 μM). Still, it was observed that the existence of these agents did not give rise to any noteworthy interfering effect throughout the assessment of histamine. There is 1 to 4% [relative standard deviation (% RSD)] change detected in the current. Thus, the prepared WS_2/CS/SPE electrode recommends its applicable selectivity concerning the concurrent verification of histamine in the existence of various amines. The standards of oxidation peak current were noted to decrease by 2.94, 3.27, 2.14, 3.16, and 2.67%, with the addition of cysteine, glycine, methionine, phenylalanine, and tryptophan, respectively [the corresponding table shown in Table S5]. The WS_2/CS/SPE-modified electrodes are accustomed to selectively govern histamine in the presence of interferents, improve surface affinity for histamine, optimize nanocomposite size and shape for proficient adsorption of histamine, and quite control experimental terms consistent with pH and temperature.

3.7.8. Real Sample Analysis of Histamine on the WS_2/CS/SPE Electrode. It is important to note that histamine levels vary widely depending on the processing, storage contexts, and specific type of food. Histamine widely exists in diverse food items, particularly those that go through fermentation or aging processes such as cheese (CH), tomato sauce (TS), tomato ketchup (TK), soy sauce (SS), etc. Additionally, histamine intolerance is a condition in which individuals are sensitive to even low levels of histamine, leading to symptoms such as headaches, hives, and gastrointestinal issues. People with histamine intolerance must be cautious about consuming foods high in histamine. The quantity of histamine in various food samples indicates the freshness of the food sample. Here, we demonstrate the histamine concentration in some real samples and its calibration bar graph shown in Figure 5e [the corresponding table shown in Table S6 as well as corresponding CV curves in Figure S4b].

4. CONCLUSIONS

We presented an efficient method for synthesizing WS_2 nanosheets. The SPE was fabricated through an effortless drop-casting technique with WS_2 and, after that, with CS. From the scan rate analysis, we estimated that the K_s, γ, and D of the WS_2/CS/SPE electrode are 0.395 s^{-1}, 1.78×10^{-8} mol cm^{-2}, and 1.03×10^{-2} cm^2 s^{-1}, respectively. The EIS plot estimates R_{ct} values of 554.77, 39.967, and 11.789 Ω for the bare SPE, WS_2/SPE, and WS_2/CS/SPE, respectively. The charge transfer rate constant calculated from EIS for the bare SPE, WS_2/SPE, and WS_2/CS/SPE are 7.54×10^{-4}, 7.98×10^{-3}, and 2.18×10^{-2} cm s^{-1}, respectively. Through electrochemical studies, we demonstrate the diverse biosensing aspects, particularly a response time of 15 s, sensitivity of 1.44×10^{-4} mA/μM cm^2, and LoD of 0.0844 μM. Furthermore, good response stability as well as reproducibility were described, which attributed to reliable histamine sensing. This research will pave the path for the enhancement of histamine sensors through quick, safe, and economical procedures with higher detection quality in the future.

https://doi.org/10.1021/acsomega.4c10419
ACS Omega 2025, 10, 3153−3164

■ ASSOCIATED CONTENT

Supporting Information

The Supporting Information is available free of charge at https://pubs.acs.org/doi/10.1021/acsomega.4c10419.

Scan rate analysis of the bare SPE electrode and WS_2/CS/SPE electrode, response time analysis, reusability analysis, stability analysis, interference analysis, and real sample analysis of the histamine on the WS_2/CS/SPE electrode, XRD spectrum of the bare glass material, SEM images of the bare SPE and the synthesized WS_2 nanosheet, CV curves from the interference study of histamine and Real sample analysis of histamine on the WS_2/CS/SPE electrode, and XPS survey spectrum of WS_2, W 4f spectra, and S 2p spectra before and after the charging effect (PDF)

■ AUTHOR INFORMATION

Corresponding Author

Jay Singh − *Department of Chemistry, Institute of Sciences, Banaras Hindu University, Varanasi, Uttar Pradesh 221005, India;* orcid.org/0000-0002-3793-0450; Phone: +91-9871766453; Email: jaysingh.chem@bhu.ac.in, jaimnnit@gmail.com

Authors

Diksha Singh − *Department of Chemistry, Institute of Sciences, Banaras Hindu University, Varanasi, Uttar Pradesh 221005, India*

Ankur Srivastava − *Department of Chemistry, Institute of Sciences, Banaras Hindu University, Varanasi, Uttar Pradesh 221005, India*

Vivek K. Chaturvedi − *Department of Gastroenterology, Institute of Medical Sciences, Banaras Hindu University, Varanasi, Uttar Pradesh 211302, India*

Complete contact information is available at: https://pubs.acs.org/10.1021/acsomega.4c10419

Author Contributions

Data curation, investigation, visualization, writing−original draft. A.S.: data curation, validation, writing−original draft. V.K.C.: data curation, validation. J.S.: conceptualization, resources, validation, project administration, supervision, writing review and editing of the original draft.

Funding

This work received no specific grant from public, commercial, or not-for-profit funding agencies.

Notes

The authors declare no competing financial interest.

■ ACKNOWLEDGMENTS

D.S. acknowledges CSIR, New Delhi, for financial assessment under the program CSIR- 09/0013(17524)/2024-EMR-I. A.S. is thankful to BHU for funding during this work. V.K.C. acknowledges ICMR, New Delhi, for providing financial support. J.S. acknowledges BHU for offering a seed grant along with a bridge grant under MoE Govt. India, Institute of Eminence (IoE), under Dev. Scheme No. 6031 7 6031A.

■ REFERENCES

(1) Gagic, M.; Jamroz, E.; Krizkova, S.; Milosavljevic, V.; Kopel, P.; Adam, V. Current Trends in Detection of Histamine in Food and Beverages. *J. Agric. Food Chem.* **2019**, *67* (3), 773−783.

(2) Halász, A.; Baráth, Á.; Simon-Sarkadi, L.; Holzapfel, W. Biogenic amines and their production by microorganisms in food. *Trends Food Sci. Technol.* **1994**, *5* (2), 42−49.

(3) Puthongkham, P.; Lee, S. T.; Venton, B. J. Mechanism of Histamine Oxidation and Electropolymerization at Carbon Electrodes. *Anal. Chem.* **2019**, *91* (13), 8366−8373.

(4) Xu, X.; Wu, X.; Ding, Y.; Zhou, X. Multicolorimetric sensing of histamine in fishes based on enzymatic etching of gold nanorods. *Food Control* **2021**, *127*, No. 108143.

(5) Li, S.; Zhong, T.; Long, Q.; Huang, C.; Chen, L.; Lu, D.; Li, X.; Zhang, Z.; Shen, G.; Hou, X. A gold nanoparticles-based molecularly imprinted electrochemical sensor for histamine specific-recognition and determination. *Microchem. J.* **2021**, *171*, No. 106844.

(6) Jiang, S.; Peng, Y.; Ning, B.; Bai, J.; Liu, Y.; Zhang, N.; Gao, Z. Surface plasmon resonance sensor based on molecularly imprinted polymer film for detection of histamine. *Sensors Actuators B Chem.* **2015**, *221*, 15−21.

(7) Poolakkandy, R. R.; Menamparambath, M. M. Transition metal oxide based non-enzymatic electrochemical sensors: An arising approach for the meticulous detection of neurotransmitter biomarkers. *Electrochem. Sci. Adv.* **2021**, *1* (2), No. e2000024.

(8) Lehane, L.; Olley, J. Histamine fish poisoning revisited. *Int. J. Food Microbiol.* **2000**, *58* (1−2), 1−37.

(9) Maintz, L.; Novak, N. Histamine and histamine intolerance. *Am. J. Clin. Nutr.* **2007**, *85* (5), 1185−1196.

(10) Latorre-Moratalla, M. L.; Veciana-Nogués, T.; Bover-Cid, S.; Garriga, M.; Aymerich, T.; Zanardi, E.; Ianieri, A.; Fraqueza, M. J.; Patarata, L.; Drosinos, E. H.; Lauková, A.; Talon, R.; Vidal-Carou, M. C. Biogenic amines in traditional fermented sausages produced in selected European countries. *Food Chem.* **2008**, *107* (2), 912−921.

(11) Stojanović, Z. S.; Mehmeti, E.; Kalcher, K.; Guzsvány, V.; Stanković, D. M. SWCNT-modified carbon paste electrode as an electrochemical sensor for histamine determination in alcoholic beverages. *Food Anal. Methods* **2016**, *9* (10), 2701−2710.

(12) Rauscher-Gabernig, E.; Grossgut, R.; Bauer, F.; Paulsen, P. Assessment of alimentary histamine exposure of consumers in Austria and development of tolerable levels in typical foods. *Food Control* **2009**, *20* (4), 423−429.

(13) U.S. Department of Health and Human Services, Food and Drug Administration, Center for Food Safety and Applied Nutrition*Fish and Fishery Products Hazards and Controls Guidance* June 2022 ed.; 2022. .

(14) Kalač, P.; Křížek, M. Formation of biogenic amines in four edible mushroom species stored under different conditions. *Food Chem.* **1997**, *58* (3), 233−236.

(15) Shalaby, A. R. Significance of biogenic amines to food safety and human health. *Food Res. Int.* **1996**, *29* (7), 675−690.

(16) Santos, M. H. S. Biogenic amines: their importance in foods. *Int. J. Food Microbiol.* **1996**, *29* (2−3), 213−231.

(17) Bodmer, S.; Imark, C.; Kneubühl, M. Biogenic amines in foods: Histamine and food processing. *Inflamm. Res.* **1999**, *48* (6), 296−300.

(18) Jastrzębska, A.; Kurzawa, M.; Piasta, A.; Szłyk, E. Determination of Histamine in Some Foods by Isotachophoretic Method with Simple Sample Preparation. *Food Anal. Methods* **2012**, *5* (5), 1079−1087.

(19) López-Sabater, E. I.; Rodríguez-Jerez, J. J.; Roig-Sagués, A. X.; Teresa Mora-Ventura, M. A. Bacteriological Quality of Tuna Fish (Thunnus thynnus) Destined for Canning: Effect of Tuna Handling on Presence of Histidine Decarboxylase Bacteria and Histamine Level. *J. Food Prot.* **1994**, *57* (4), 318−323.

(20) Serrano, V. M.; Cardoso, A. R.; Diniz, M.; Sales, M. G. F. In-situ production of Histamine-imprinted polymeric materials for electrochemical monitoring of fish. *Sensors Actuators B Chem.* **2020**, *311*, No. 127902.

(21) Valenta, R.; Hochwallner, H.; Linhart, B.; Pahr, S. Food Allergies: The Basics. *Gastroenterology* **2015**, *148* (6), 1120−1131.

(22) Rodriguez, R. S.; O'Keefe, T. L.; Froehlich, C.; Lewis, R. E.; Sheldon, T. R.; Haynes, C. L. Sensing Food Contaminants: Advances in Analytical Methods and Techniques. *Anal. Chem.* **2021**, *93* (1), 23−40.

(23) Odeyemi, O. A. Public health implications of microbial food safety and foodborne diseases in developing countries. *Food Nutr. Res.* **2016**, *60* (1), 29819.
(24) Munir, M. A.; Mackeen, M. M. M.; Heng, L. Y.; Badri, K. H. Study of Histamine Detection using Liquid Chromatography and Gas Chromatography. *ASM Sci. J.* **2021**, *16*, 1−9.
(25) Krittanawong, C.; Isath, A.; Hahn, J.; Wang, Z.; Narasimhan, B.; Kaplin, S. L.; Jneid, H.; Virani, S. S.; Tang, W. H. W. Fish Consumption and Cardiovascular Health: A Systematic Review. *Am. J. Med.* **2021**, *134* (6), 713−720.
(26) Kounnoun, A.; EL Maadoudi, M.; Cacciola, F.; Mondello, L.; Bougtaib, H.; Alahlah, N.; Amajoud, N.; EL Baaboua, A.; Louajri, A. Development and Validation of a High-Performance Liquid Chromatography Method for the Determination of Histamine in Fish Samples Using Fluorescence Detection with Pre-column Derivatization. *Chromatographia* **2020**, *83* (7), 893−901.
(27) Antoine, F. R.; Wei, C.; Otwell, W. S.; Sims, C. A.; Littell, R. C.; Hogle, A. D.; Marshall, M. R. Gas Chromatographic Analysis of Histamine in Mahi-mahi (Coryphaena hippurus). *J. Agric. Food Chem.* **2002**, *50* (17), 4754−4759.
(28) Hwang, B.-S.; Wang, J.-T.; Choong, Y.-M. A rapid gas chromatographic method for the determination of histamine in fish and fish products. *Food Chem.* **2003**, *82* (2), 329−334.
(29) Ough, C. S. Measurement of histamine in California wines. *J. Agric. Food Chem.* **1971**, *19* (2), 241−244.
(30) Numanoğlu, E.; Boyaci, I. H.; Topcu, A. Simple determination of histamine in cheese by capillary electrophoresis with diode array detection. *J. Food Drug Anal.* **2008**, *16* (6), 74.
(31) Tamim, N. M.; Bennett, L. W.; Shellem, T. A.; Doerr, J. A. High-Performance Liquid Chromatographic Determination of Biogenic Amines in Poultry Carcasses. *J. Agric. Food Chem.* **2002**, *50* (18), 5012−5015.
(32) Romero-González, R.; Alarcón-Flores, M. I.; Vidal, J. L. M.; Frenich, A. G. Simultaneous Determination of Four Biogenic and Three Volatile Amines in Anchovy by Ultra-High-Performance Liquid Chromatography Coupled to Tandem Mass Spectrometry. *J. Agric. Food Chem.* **2012**, *60* (21), 5324−5329.
(33) Young, J. A.; Jiang, X.; Kirchhoff, J. R. Amperometric Detection of Histamine with a Pyrroloquinoline-Quinone Modified Electrode. *Electroanalysis* **2013**, *25* (7), 1589−1593.
(34) Pérez, S.; Bartrolí, J.; Fàbregas, E. Amperometric biosensor for the determination of histamine in fish samples. *Food Chem.* **2013**, *141* (4), 4066−4072.
(35) Munir, M. A.; Badri, K. H.; Heng, L. Y.; Mackeen, M. M. M.; Sage, E. E. Histamine Detection in Mackerel (Scomberomorus Sp.) and its Products Derivatized with 9-Flourenilmethylchloroformate. *Pakistan J. Anal. Environ. Chem.* **2021**, *22* (2), 243−251.
(36) Yu, X.; Zhong, T.; Zhang, Y.; Zhao, X.; Xiao, Y.; Wang, L.; Liu, X.; Zhang, X. Design, Preparation, and Application of Magnetic Nanoparticles for Food Safety Analysis: A Review of Recent Advances. *J. Agric. Food Chem.* **2022**, *70* (1), 46−62.
(37) Renedo, O. D.; Alonso-Lomillo, M. A.; Martínez, M. J. A. Recent developments in the field of screen-printed electrodes and their related applications. *Talanta* **2007**, *73* (2), 202−219.
(38) Zha, X.; Sun, W.; Liu, J.; Sun, G.; Lu, S.; Wang, Y. Three-dimensional hydrangea-like layered double hydroxide anchoring hollow metal organic-framework for efficient adsorption of 2, 4-dichlorophenoxyacetic acid. *Mater. Today Chem.* **2024**, *35*, No. 101883.
(39) Lu, S.; Wang, Q.; Fang, L.; Zheng, X.; Yin, F.; Liu, H. Bimetallic Platinum−Nickel Nanoparticles Modified on the Screen-Printed Electrode for Highly Sensitive Urea Determination. *IEEE Sens. J.* **2024**, *24* (4), 4221−4227.
(40) Hu, W.-W.; Chen, Z. Role of Histamine and Its Receptors in Cerebral Ischemia. *ACS Chem. Neurosci.* **2012**, *3* (4), 238−247.
(41) Meng, X.; Dong, X.; Liu, D.; Niu, Q.; Lu, S.; You, T. Rapid Electrochemical Sensing of Zn(II) Using MesoporousMnO 2 @N-Graphene Composites. *IEEE Sens. J.* **2023**, *23* (21), 25673−25679.
(42) Alagh, A.; Annanouch, F. E.; Umek, P.; Bittencourt, C.; Sierra-Castillo, A.; Haye, E.; Colomer, J. F.; Llobet, E. CVD growth of self-assembled 2D and 1D WS2 nanomaterials for the ultrasensitive detection of NO2. *Sensors Actuators B Chem.* **2021**, *326*, No. 128813.
(43) Chia, X.; Eng, A. Y. S.; Ambrosi, A.; Tan, S. M.; Pumera, M. Electrochemistry of Nanostructured Layered Transition-Metal Dichalcogenides. *Chem. Rev.* **2015**, *115* (21), 11941−11966.
(44) Pumera, M.; Loo, A. H. Layered transition-metal dichalcogenides (MoS2 and WS2) for sensing and biosensing. *TrAC Trends Anal. Chem.* **2014**, *61*, 49−53.
(45) Lu, S.; Xiang, S.; Wang, C.; Liu, H. Carbon nanotubes decorated with bimetallic PtCo nanoparticles for sensitive detection of uric acid. *Electrochem. commun.* **2024**, *166*, No. 107774.
(46) Yu, Y.; Zhang, Y.; Song, X.; Zhang, H.; Cao, M.; Che, Y.; Dai, H.; Yang, J.; Zhang, H.; Yao, J. PbS-Decorated WS 2 Phototransistors with Fast Response. *ACS Photonics* **2017**, *4* (4), 950−956.
(47) Manna, S.; Seth, A.; Gupta, P.; Nandi, G.; Dutta, R.; Jana, S.; Jana, S. Chitosan Derivatives as Carriers for Drug Delivery and Biomedical Applications. *ACS Biomater. Sci. Eng.* **2023**, *9* (5), 2181−2202.
(48) Marangon, C. A.; Martins, V. C. A.; Ling, M. H.; Melo, C. C.; Plepis, A. M. G.; Meyer, R. L.; Nitschke, M. Combination of Rhamnolipid and Chitosan in Nanoparticles Boosts Their Antimicrobial Efficacy. *ACS Appl. Mater. Interfaces* **2020**, *12* (5), 5488−5499.
(49) Desbrières, J.; Guibal, E. Chitosan for wastewater treatment. *Polym. Int.* **2018**, *67* (1), 7−14.
(50) Yuan, Y.; Li, R.; Liu, Z. Establishing Water-Soluble Layered WS 2 Nanosheet as a Platform for Biosensing. *Anal. Chem.* **2014**, *86* (7), 3610−3615.
(51) Madhurantakam, S.; Karnam, J. B.; Brabazon, D.; Takai, M.; Ahad, I. U.; Balaguru Rayappan, J. B.; Krishnan, U. M. Nano": An Emerging Avenue in Electrochemical Detection of Neurotransmitters. *ACS Chem. Neurosci.* **2020**, *11* (24), 4024−4047.
(52) Liu, J.; Cao, Y. An electrochemical sensor based on an anti-fouling membrane for the determination of histamine in fish samples. *Anal. Methods* **2021**, *13* (5), 685−694.
(53) Patterson, A. L. The Scherrer Formula for X-Ray Particle Size Determination. *Phys. Rev.* **1939**, *56* (10), 978−982.
(54) Yin, W.; Bai, X.; Chen, P.; Zhang, X.; Su, L.; Ji, C.; Gao, H.; Song, H.; Yu, W. W. Rational Control of Size and Photoluminescence of WS 2 Quantum Dots for White Light-Emitting Diodes. *ACS Appl. Mater. Interfaces* **2018**, *10* (50), 43824−43830.
(55) Verma, A.; Yadav, B. C. 2D/2D Nanostructured System Based on WO 3 /WS 2 for Acetone Sensor and Breath Analyzer. *ACS Appl. Nano Mater.* **2023**, *6* (7), 5493−5507.
(56) Huang, C.-C.; Wang, H.; Cao, Y.; Weatherby, E.; Richheimer, F.; Wood, S.; Jiang, S.; Wei, D.; Dong, Y.; Lu, X.; Wang, P.; Polcar, T.; Hewak, D. W. Facilitating Uniform Large-Scale MoS 2, WS 2 Monolayers, and Their Heterostructures through van der Waals Epitaxy. *ACS Appl. Mater. Interfaces* **2022**, *14* (37), 42365−42373.
(57) Lee, N.; Shin, M.-H.; Lee, E.; Cho, S.-H.; Hwang, H.; Cho, K.; Kim, J. K.; Hahn, S. K. Three-Dimensional Tungsten Disulfide Raman Biosensor for Dopamine Detection. *ACS Appl. Bio Mater.* **2020**, *3* (11), 7687−7695.
(58) Mao, X.; Xu, Y.; Xue, Q.; Wang, W.; Gao, D. Ferromagnetism in exfoliated tungsten disulfide nanosheets. *Nanoscale Res. Lett.* **2013**, *8* (1), 430.
(59) Govindarajan, N.; Xu, A.; Chan, K. How pH affects electrochemical processes. *Science (80-.)* **2022**, *375* (6579), 379−380.
(60) Elgrishi, N.; Rountree, K. J.; McCarthy, B. D.; Rountree, E. S.; Eisenhart, T. T.; Dempsey, J. L. A Practical Beginner's Guide to Cyclic Voltammetry. *J. Chem. Educ.* **2018**, *95* (2), 197−206.
(61) Klingler, R. J.; Kochi, J. K. Electron-transfer kinetics from cyclic voltammetry. Quantitative description of electrochemical reversibility. *J. Phys. Chem.* **1981**, *85* (12), 1731−1741.
(62) Wang, H.; Sayed, S. Y.; Luber, E. J.; Olsen, B. C.; Shirurkar, S. M.; Venkatakrishnan, S.; Tefashe, U. M.; Farquhar, A. K.; Smotkin, E. S.; McCreery, R. L.; Buriak, J. M. Redox Flow Batteries: How to Determine Electrochemical Kinetic Parameters. *ACS Nano* **2020**, *14* (3), 2575−2584.

https://doi.org/10.1021/acsomega.4c10419
ACS Omega 2025, 10, 3153−3164

(63) Laviron, E. General expression of the linear potential sweep voltammogram in the case of diffusionless electrochemical systems. *J. Electroanal. Chem. Interfacial Electrochem.* **1979**, *101* (1), 19−28.
(64) Singh, J.; Singh, K. R.; Kumar, M.; Verma, R.; Verma, R.; Malik, P.; Srivastava, S.; Singh, R. P.; Kumar, D. Melt-quenched vanadium pentoxide-stabilized chitosan nanohybrids for efficient hydrazine detection. *Mater. Adv.* **2021**, *2* (20), 6665−6675.
(65) Verma, R.; Singh, K. R.; Verma, R.; Singh, J. Electro-optical behaviour of CuFe 2 O 4 @rGO nanocomposite for nonenzymatic detection of uric acid via the electrochemical method. *Luminescence* **2023**, *38*, 1393.
(66) Brown, A. P.; Anson, F. C. Cyclic and differential pulse voltammetric behavior of reactants confined to the electrode surface. *Anal. Chem.* **1977**, *49* (11), 1589−1595.
(67) Singh, D.; Shaktawat, S.; Yadav, S. K.; Verma, R.; Singh, K. R. B.; Singh, J. Chitosan-assisted self-assembly of flower-shaped ε-Fe2O3 nanoparticles on screen-printed carbon electrode for Impedimetric detection of Cd2+, Pb2+, and Hg2+ heavy metal ions in various water samples. *Int. J. Biol. Macromol.* **2024**, *265*, No. 130867.
(68) Nontipichet, N.; Khumngern, S.; Choosang, J.; Thavarungkul, P.; Kanatharana, P.; Numnuam, A. An enzymatic histamine biosensor based on a screen-printed carbon electrode modified with a chitosan−gold nanoparticles composite cryogel on Prussian blue-coated multi-walled carbon nanotubes. *Food Chem.* **2021**, *364*, No. 130396.
(69) Gumpu, M. B.; Nesakumar, N.; Sethuraman, S.; Krishnan, U. M.; Rayappan, J. B. B. Development of electrochemical biosensor with ceria−PANI core−shell nano-interface for the detection of histamine. *Sensors Actuators B Chem.* **2014**, *199*, 330−338.

https://doi.org/10.1021/acsomega.4c10419
ACS Omega 2025, 10, 3153−3164